The Journal of Experimental Biology 213, 621-634

doi:10.1242/jeb.032631

Kinematics and hydrodynamics analysis of swimming anurans reveals striking inter-specific differences in the mechanism for producing thrust

Christopher T. Richards
The Rowland Institute at Harvard, Harvard University, Cambridge, MA 02142, USA
richards@fas.harvard.edu

Accepted 9 November 2009

SUMMARY

This study aimed to compare the swimming kinematics and hydrodynamics within and among aquatic and semi-aquatic/terrestrial frogs. High-speed video was used to obtain kinematics of the leg joints and feet as animals swam freely across their natural range of speeds. Blade element analysis was then used to model the hydrodynamic thrust as a function of foot kinematics. Two purely aquatic frogs, *Xenopus laevis* and *Hymenochirus boettgeri*, were compared with two semi-aquatic/terrestrial frogs, *Rana pipiens* and *Bufo americanus*. The four species performed similarly. Among swimming strokes, peak stroke velocity ranged from 3.3±1.1 to 20.9±2.5, from 6.8±2.1 to 28.6±3.7 and from 4.9±0.5 to 20.9±4.1 body lengths per second (BL s^{-1}) in *X. laevis*, *H. boettgeri* and *R. pipiens*, respectively (means ± s.d.; *N*=4 frogs for each). *B. americanus* swam much more slowly at 3.1±0.3 to 7.0±2.0 BL s^{-1} (*N*=3 frogs). Time-varying joint kinematics patterns were superficially similar among species. Because foot kinematics result from the cumulative motion of joints proximal to the feet, small differences in time-varying joint kinematics among species resulted in species-specific foot kinematics (therefore hydrodynamics) patterns. To obtain a simple measure of the hydrodynamically useful motion of the foot, this study uses 'effective foot velocity' (*EFV*): a measure of the component of foot velocity along the axis of swimming. Resolving *EFV* into translational and rotational components allows predictions of species-specific propulsion strategies. Additionally, a novel kinematic analysis is presented here that enables the partitioning of translational and rotational foot velocity into velocity components contributed by extension at each individual limb joint. Data from the kinematics analysis show that *R. pipiens* and *B. americanus* translated their feet faster than their body moved forward, resulting in positive net translational *EFV*. Conversely, translational *EFV* was slower than the body velocity in *H. boettgeri* and *X. laevis*, resulting in negative net translational *EFV*. Consequently, the translational component of thrust (caused mostly by hip, knee and ankle extension) was twofold higher than rotational thrust in *Rana pipiens*. Likewise, rotational components of thrust were nearly twofold higher than translational components in *H. boettgeri*. *X. laevis*, however, was the most skewed species observed, generating nearly 100% of total thrust by foot rotation generated by hip, ankle and tmt extension. Thus, this study presents a simple kinematics analysis that is predictive of hydrodynamic differences among species. Such differences in kinematics reveal a continuum of different propulsive strategies ranging from mostly rotation-powered (*X. laevis*) to mostly translation-powered (*R. pipiens*) swimming.

Supplementary material available online at http://jeb.biologists.org/cgi/content/full/213/4/621/DC1

Key words: blade element model, Bufonidae, hydrodynamics, kinematics, Pipidae, Ranidae.

INTRODUCTION

For decades, frogs have served as model systems to understand the link between morphology and performance. For example, the morphological and ecological variety of frogs has generated much interest in how musculoskeletal anatomy relates to diversity in jumping performance among species (Rand, 1952; Emerson, 1978; Zug, 1978). More recently, single species studies of jumping mechanics have relied on the rich body of anuran muscle physiology work (Hill, 1970) to establish an integrated understanding of the limits of jumping performance in the context of muscle mechanics (Lutz and Rome, 1994; Peplowski and Marsh, 1997; Roberts and Marsh, 2003). Such studies have led to exploration of the unique demands of terrestrial *versus* aquatic locomotion met through modulating motor control (Peters et al., 1996; Gillis and Biewener, 2000) and the propulsive impulse from the hind limbs (Nauwelaerts and Aerts, 2003). Furthermore, species that are both excellent swimmers and jumpers potentially have musculoskeletal compromises that benefit swimming at the expense of jumping performance [and *vice versa* (Nauwelaerts et al., 2007)]. However, despite much comparative work on jumping frogs, there are no studies comparing the swimming mechanics of 'generalized' semi-aquatic species with either 'specialized' jumpers or swimmers. The current study combines previously developed analytical tools (Gal and Blake, 1988; Nauwelaerts and Aerts, 2003; Richards, 2008) with novel approaches to investigate the hind limb kinematics and hydrodynamics of two aquatic species (*Xenopus laevis* and *Hymenochirus boettgeri*) compared with the semi-aquatic *Rana pipiens* and the terrestrial *Bufo americanus*.

In addition to exploring the relationship between morphology and function, frogs are ideal models for addressing the link between kinematics and performance. Similar to other tetrapods, anuran hind limbs have joints that enable a large range of various leg kinematics patterns (Kargo and Rome, 2002). In principle, any individual frog may vary its limb kinematics within this potential limb 'workspace' [e.g. to achieve different swimming speeds (Richards, 2008)]. Likewise, an entire species may use a particular set of kinematics

(within the workspace) according to the species' required range of swimming tasks. For example, an ambush predator that feeds in the water may use a different set of kinematics from a semi-aquatic frog that only enters the water to dive to the bottom upon escaping predation. Previous workers have established that use of synchronous leg motions produces higher thrust and faster swimming speed than kicking the legs asynchronously (Johansson and Lauder, 2004). However, variation in time-varying kinematics patterns (within an individual frog) has only been measured in detail for two species, *Rana esculenta* (Nauwelaerts and Aerts, 2003) and *X. laevis* (Richards, 2008). Moreover, hind limb kinematics during synchronous swimming have been suggested to be species specific (Johansson and Lauder, 2004), motivating the current study, which investigates the kinematic diversity of synchronous swimming kicks among anurans.

Given the diversity of available kinematics patterns within individuals and among species, attempting to relate the many joint kinematics parameters (e.g. joint extension amplitudes, phases and velocities) is potentially difficult. In the current study, I use a recently developed method for decomposing foot motion into aft-directed translational velocity and cranio-caudal foot rotational velocity (Richards, 2008) to relate time-varying joint kinematics to foot kinematics and hydrodynamic performance. Prior work on ranid frogs suggests that the feet generate propulsion mainly by translation. Although neither measurements of translational *versus* rotational velocity nor hydrodynamic modeling have been done, workers have observed that the feet are held at 90 deg. to flow during power strokes (Peters et al., 1996; Johansson and Lauder, 2004; Nauwelaerts et al., 2005). Nauwelaerts et al. speculated that a ranid foot may be biased toward translational motion because of a higher moment of inertia (Nauwelaerts et al., 2007). Consequently, strong jumpers may be expected to have a high foot moment of inertia (relative to fully aquatic species) in order to maximize the period of ground contact during jumps. By contrast, *X. laevis* were found to produce thrust mostly by rapid foot rotation, with foot translation contributing much less significantly to total thrust impulse (Richards, 2008). Similarly, the aquatic *H. boettgeri* rotate their feet continuously throughout the stroke, unlike *R. pipiens*, which maintain the feet nearly perpendicular to flow [e.g. compare fig. 5B from Gal and Blake (Gal and Blake, 1988) to fig. 4 from Peters et al. (Peters et al., 1996)]. I therefore suggest that rotational velocity is important for both *X. laevis* and *H. boettgeri*.

Based on prior work, the current study uses kinematics and hydrodynamic modeling to test the hypothesis that purely aquatic species, *Xenopus laevis* and *Hymenochirus boettgeri* (belonging to Pipidae), generate thrust by foot rotation, and semi-aquatic (or terrestrial) species, *Rana pipiens* (Ranidae) and *Bufo americanus* (Bufonidae), generate propulsion mainly by foot translation. The current study is the first detailed comparative analysis of the hydrodynamic mechanism of swimming among frog species and within individuals of a given species. Findings will give insight into how individual frogs operate within the anuran 'kinematics workspace'. Moreover, the analysis will reveal that kinematic variation is species specific. Additionally, methods introduced in the current study will provide an analytical framework for integrating joint kinematics and hydrodynamics to help understand the function of multi-joint limbs during swimming.

MATERIALS AND METHODS

Animals

Xenopus laevis (Daudin 1802) were obtained from Xenopus Express, Inc. (Plant City, FL, USA). *Rana pipiens* (Schreber 1782) and *Hymenochirus boettgeri* (Tornier 1896) were purchased from Carolina Biological (Burlington, NC, USA). *Bufo americanus* (Holbrook 1836) toads were wild-caught in Bedford, MA, USA. All frogs were housed in aquaria at the Concord Field Station and maintained at 20–22°C under a 12 h:12 h light:dark cycle.

Kinematics and high-speed video

Small (~0.5 cm diameter) plastic markers were placed on the skin above the snout, hip, knee, ankle and tarsometatarsal (tmt) joints (Fig. 1A) using a cyanoacrylate adhesive. Frogs were filmed from above swimming in a still water tank (27×52 cm Plexiglas^{TM} for *H. boettgeri* and 80 cm×96 cm Plexiglas^{TM} for all other species) at 250 frames s^{-1} at a 1/1000 s shutter speed with a high-speed Photron Fastcam camera (Photron Ltd, San Diego, CA, USA). Each swimming tank was large enough for several swimming strokes (roughly 6, 17, 7, 14 swimming strokes for *X. laevis*, *H. boettgeri*, *R. pipiens* and *B. americanus*, respectively). Due to behavioral differences between species, *R. pipiens* and *B. americanus* were filmed swimming at the surface, whereas *X. laevis* and *H. boettgeri* swam submerged. For *X. laevis* and *H. boettgeri*, a water depth of 5–6 cm was used to ensure horizontal swimming. For *R. pipiens* and *B. americanus*, deeper water (~20 cm) was used to avoid hydrodynamic interactions between the feet and the bottom. *X*–*Y* marker coordinates were digitized in Matlab (The MathWorks, Natick, MA, USA) using a customized routine (DLTdataviewer 2.0 written by Tyson Hedrick). To obtain foot angle measurements, the position of the tip of the second toe was digitized in addition to the joint markers. Only synchronous strokes with a straight swimming trajectory were analyzed. A range of slow to fast swimming sequences was elicited by tapping slightly behind the frog leg. Several swimming sequences were recorded to capture the entire range of swimming velocities. Only the power stroke (i.e. defined as the period of positive center of mass acceleration) was analyzed for each swimming stroke (Fig. 1B; see Discussion).

Joint kinematics calculations

Data traces of joint *X*–*Y* coordinates were smoothed using a second-order forward–backward 20 Hz low-pass Butterworth filter before computing joint angles (Fig. 1A). All data processing and calculations were done in Labview 7.1 (National Instruments, Austin, TX, USA). Since frogs swam freely in the global coordinate space, velocity components of the feet needed to be calculated in a local coordinate system defined as the snout–vent axis (X) and the medio-lateral axis (Y) originating at the animal's vent (Fig. 1A). I used the following equations to derive foot velocity components directly from joint angles, independent of the frog's orientation in global coordinates:

$$\mathbf{d}_{t,hip} = L_{fem}\cos(\pi - \theta_{hip}), \quad (1)$$

$$\mathbf{d}_{t,knee} = L_{tib}\cos(\theta_{hip} - \theta_{knee}), \quad (2)$$

$$\mathbf{d}_{t,ankle} = L_{tars}\cos(\pi - \theta_{hip} + \theta_{knee} - \theta_{ankle}), \quad (3)$$

$$\mathbf{d}_{t} = \mathbf{d}_{t,hip} + \mathbf{d}_{t,knee} + \mathbf{d}_{t,ankle}, \quad (4)$$

where θ_{hip}, θ_{knee} and θ_{ankle} are joint angles (in radians) and $\mathbf{d}_{t,hip}$, $\mathbf{d}_{t,knee}$ and $\mathbf{d}_{t,ankle}$ are hip, knee and ankle contributions to foot translational displacement ($\mathbf{d}_t$) with respect to the hip joint. L_{fem}, L_{tib} and L_{tars} are lengths of the femur, tibia–fibula and proximal tarsal hind limb segments (measured on the animals after experimental trials; Table 1). Time derivatives of displacements

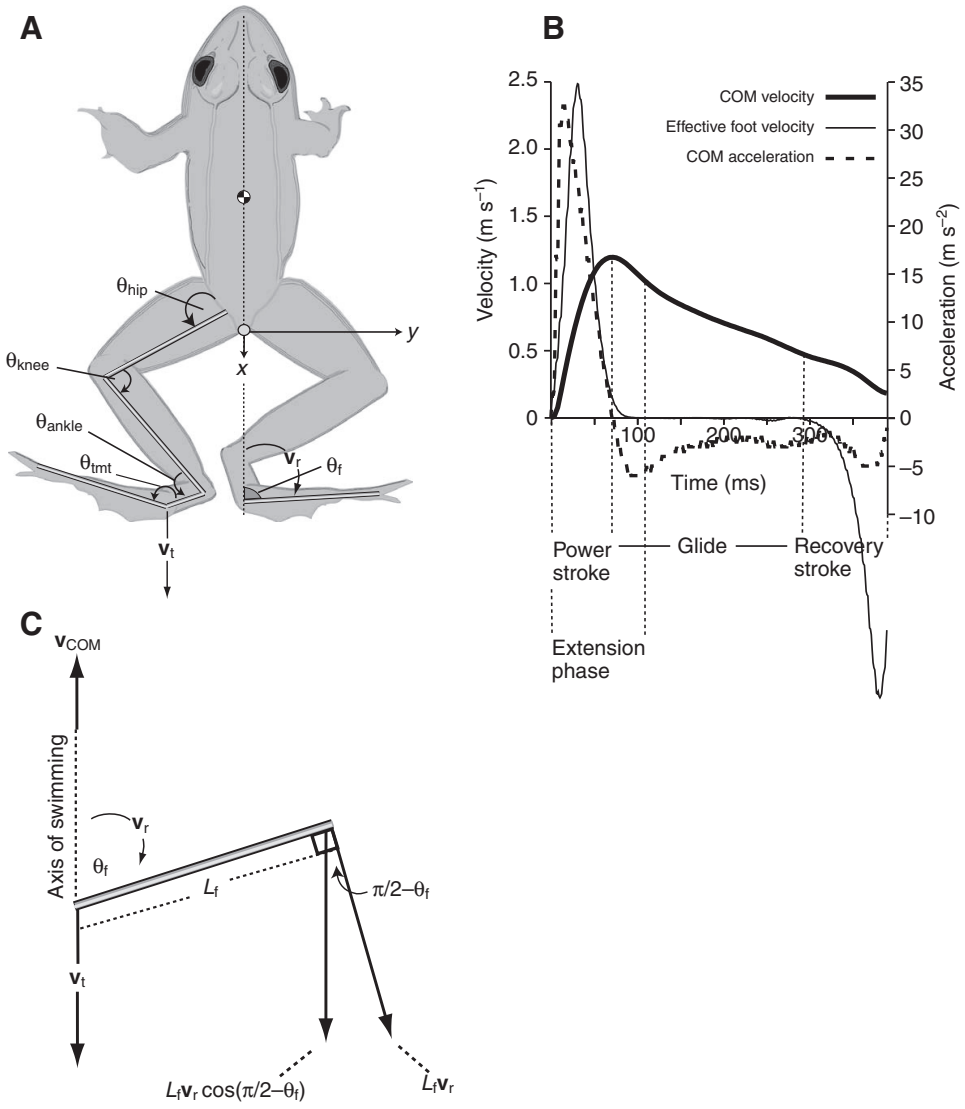

Fig. 1. General frog anatomy and swimming kinematics. (A) A tracing of *R. pipiens* showing hip (θ_{hip}), knee (θ_{knee}), ankle (θ_{ankle}), tarsometatarsal (θ_{tmt}) and foot angles (θ_f). Curved arrows indicate the direction of joint extension. Note that the joint angles are defined between adjacent leg segments whereas the foot angle is defined between the axis of swimming and the span of the foot. Translational ($\mathbf{v}_t$) and rotational ($\mathbf{v}_r$) foot velocities are relative to a local coordinate system originating at the vent (grey circle). (B) A representative swimming stroke of *X. laevis* showing center of mass (COM) velocity ($\mathbf{v}_{COM}$) (bold line), COM acceleration (broken line) and effective foot velocity (*EFV*; thin line) during the power stroke (positive COM acceleration), glide phase (the period where the legs remain extended) and recovery stroke (the period of joint flexion prior to the next swimming stroke). The extension phase (the period of positive *EFV*) is also marked. Note that the COM begins decelerating before effective foot velocity (due to joint extension) reaches zero. (C) A schematic of the right foot shows the tangential rotational velocity, ($L_f\mathbf{v}_r$), vector and its aft-directed component: $L_f\mathbf{v}_r(\cos(\pi/2-\theta_f))$, where L_f is the length of the foot. These vectors are used in the derivation of *EFV* (see Materials and methods).

yielded hip, knee and ankle velocity components ($\mathbf{v}_{t,hip}$, $\mathbf{v}_{t,knee}$ and $\mathbf{v}_{t,ankle}$) contributing to foot translational velocity ($\mathbf{v}_t$). Since translation is defined by the motion of the tmt joint (i.e. the base of the foot), tmt joint extension contributes to foot rotation but not foot translation. Lateral translational velocity ($\mathbf{v}_l$) of the feet was also considered; however $\mathbf{v}_l$ contributed only negligibly to total thrust, and, therefore, joint contributions to $\mathbf{v}_l$ are not shown in this analysis. The foot angle, θ_f, was defined in terms of all joint angles to resolve each joint's contribution to foot angular displacement ($\mathbf{d}_{r,hip}$, $\mathbf{d}_{r,knee}$, $\mathbf{d}_{r,ankle}$, $\mathbf{d}_{r,tmt}$) and rotational velocity ($\mathbf{v}_{r,hip}$, $\mathbf{v}_{r,knee}$, $\mathbf{v}_{r,ankle}$, $\mathbf{v}_{r,tmt}$):

$$\theta_f = \theta_{hip} - \theta_{knee} + \theta_{ankle} + \theta_{tmt} - \pi . \quad (5)$$

Note that θ_{knee} is negative because the angle is defined on the medial leg surface (as opposed to the lateral surface for all other joints; Fig. 1A). To measure foot velocity, translational and rotational velocity components were derived. To account for the change in the foot's projected area into flow (as the foot angle changes), the translational velocity component was calculated as:

$$\mathbf{v}_t \sin\theta_f . \quad (6)$$

The tangential rotational velocity $L_f\mathbf{v}_r$ (Gal and Blake, 1988) normal to the foot (Fig. 1C) was used to calculate the rotational velocity component along the axis of swimming:

$$L_f\mathbf{v}_r \cos(\pi/2 - \theta_f) . \quad (7)$$

Table 1. Frog morphology

	Body mass (g)	Dorso-ventral body depth (mm)	Snout–vent length (mm)	Femur length (mm)	Tibia–fibula length (mm)	Tarsal–metatarsal length (mm)	Foot length (mm)
X. laevis (*N*=4)	25.6±3.9	16±2	61±5	26±1	22±2	11±2	29±6
H. boettgeri (*N*=4)	1.2±0.3	6±0.3	24±1	9±1	7±1	4±1	8±1
R. pipiens (*N*=4)	31.6±11.1	20±3	70±8	32±3	33±1	14±1	26±3
B. americanus (*N*=3)	32.8±19.8	30±12	69±13	24±5	21±4	10±3	29±7

Values are means ± s.d.

Table 2. Joint kinematics summary

	Min. θ_{hip}	Max. θ_{hip}	Min. θ_{knee}	Max. θ_{knee}	Min. θ_{ankle}	Max. θ_{ankle}	Min. θ_{tmt}	Max. θ_{tmt}	Min. θ_f min	Max. θ_f
X. laevis	101.2±8.7^{*2}	146.9±11.8^{*3,4}	78.9±8.4^{*1,3,4}	130.9±12.4^{*3}	77.9±3.5^{*3}	152.7±6.2	134.1±7.4^{*3,4}	185.3±6.9^{*1,4}	54.2±8.1^{*2,3,4}	179.8±11.7^{*2,3,4}
H. boettgeri	85±8.8^{*1,3,4}	144.3±11.3^{*3}	37.5±6.8^{*1}	135.5±14.1^{*3}	79.9±7.9^{*3}	155.6±10.7^{*4}	131.4±10.2^{*3,4}	174.2±3^{*1,3,4}	79.3±21.8^{*1,4}	170.4±11.9^{*1}
R. pipiens	100.2±10.6^{*2}	161.3±6.2^{*1,2,4}	36±9.3^{*4}	153.7±6.9^{*1,2,4}	42.5±3.9^{*1,2,4}	162.3±6.4^{*4}	157.2±9.2^{*1,2}	184.9±4.3^{*2}	83.4±10.4^{*1,4}	168.5±4.3^{*1}
B. americanus	100.5±9.7^{*2}	140±5.1^{*1,3}	40.9±5.8^{*1}	133±3.4^{*3}	71.2±8.1^{*3}	142.7±8.6^{*2,3}	154±20.5^{*1,2}	181.3±7.5^{*1,2}	103.9±15.6^{*1,2,3}	168±2.5^{*1}

All values are means ± s.e.m for *X. laevis* (*N*=39 trials among *N*=4 frogs), *H. boettgeri* (*N*=48 trials among *N*=4 frogs), *R. pipiens* (*N*=42 trials among *N*=4 frogs) and *B. americanus* (*N*=52 trials among *N*=3 frogs). All joint angles (in deg.) are defined in Fig. 1. *Significant *P*-value (<0.05) for multiple comparisons among species 1–4 (1, *X. laevis*; 2, *H. boettgeri*; 3, *R. pipiens*; 4, *B. americanus*); e.g. ^{*2,3} indicates significant differences from *H. boettgeri* and *R. pipiens*.

I define effective foot velocity (*EFV*) as the sum of Eqn 6 and Eqn 7, representing the aft-directed component of foot velocity (for $0 \leq \theta_f \leq \pi$):

$$EFV = \sin\theta_f\,(\mathbf{v}_t + L_f\mathbf{v}_r), \quad (8)$$

where L_f is the foot length. *EFV* measures the relative contributions of translational and rotational velocity to thrust-producing foot velocity. Furthermore, to account for the backward 'slip' of the foot, net *EFV* [translational *EFV* – COM (center of mass) velocity] was calculated to obtain translational *EFV* in the global coordinate system.

Hydrodynamic modeling

Time-varying hydrodynamic thrust produced by translational and rotational velocity and acceleration of frog feet was estimated by a blade element model following earlier studies (Gal and Blake, 1988; Richards, 2008). For each species, frog body shape was approximated by an ellipsoid with axes lengths corresponding to lengths of the snout–vent, medio-lateral and dorso-ventral axes measured from individual frogs used in the video recordings. For each individual frog, digital images of feet (held flat on a sheet of Plexiglas^{TM} and photographed from below) were traced in Scion image (Scion Corporation, Frederick, MD, USA) to digitally measure foot area. Foot shape was modeled as a trapezoidal flat plate with the same area as the actual frog foot. Using a previously described and verified forward dynamics approach (Richards, 2008), these morphological measurements and foot kinematics were used to simulate time-varying hydrodynamic thrust and forward swimming velocity using a numerical differential equation solver in Mathematica 6.0 (Wolfram Research, Inc., Champaign, IL, USA). Simulated swimming COM velocity profiles (based on actual foot kinematics) were then compared with recorded COM velocity profiles to verify that the blade element model is applicable across species.

Statistics

Data for statistical analysis were gathered from measurements made on the power stroke portion of individual swimming strokes within each frog species. Multiple comparisons of means (pooled data from individual frogs) were done by ANOVA using the Tukey–Kramer HSD *post-hoc* test. Alpha values from multiple paired *t*-tests were adjusted by the sequential Bonferroni method (Quinn and Keough, 2002). Two-way ANOVAs were performed to account for variation between individual frogs when comparing means among species. For the two-way ANOVAs, species was used as a fixed factor, and individual frog was used as a random factor (nested within species). For the hydrodynamic modeling, data was split into slow swimming trials (<30% maximum swimming velocity) and fast swimming trials (>60% maximum swimming velocity). All statistical analyses were done in SPSS 16.0 (SPSS Inc., Chicago, IL, USA).

RESULTS

Swimming performance and general hind limb kinematics patterns

Each species swam by extending the hip, knee, ankle and tarsometatarsal (tmt) joints (Table 2; see Movie 1 in supplementary material). In each species, onset times of joint extension were staggered, with the knee beginning to extend first, followed by the hip then the ankle (Fig. 2). Extension onset times for the tmt and foot varied among species. Peak swimming stroke velocity in *X. laevis* ranged from 3.3±1.1 to 20.9±2.5 body lengths s^{-1} (BL s^{-1}; mean ± s.d., *N*=4 frogs). Similarly, *H. boettgeri* and *R. pipiens* peak velocities ranged from 6.8±2.1 to 28.6±3.7 BL s^{-1} (*N*=4 frogs) and from 4.9±0.5 to 20.9±4.1 BL s^{-1} (*N*=4 frogs), respectively. The velocity range of 3.1±0.3 to 7.0±2.0 BL s^{-1} for *B. americanus* was significantly narrower (*N*=4 frogs, ANOVA, Tukey–Kramer, $P \leq 0.01$) than the other species. The velocity ranges of the three other species did not differ significantly ($P > 0.2$). Joint kinematics

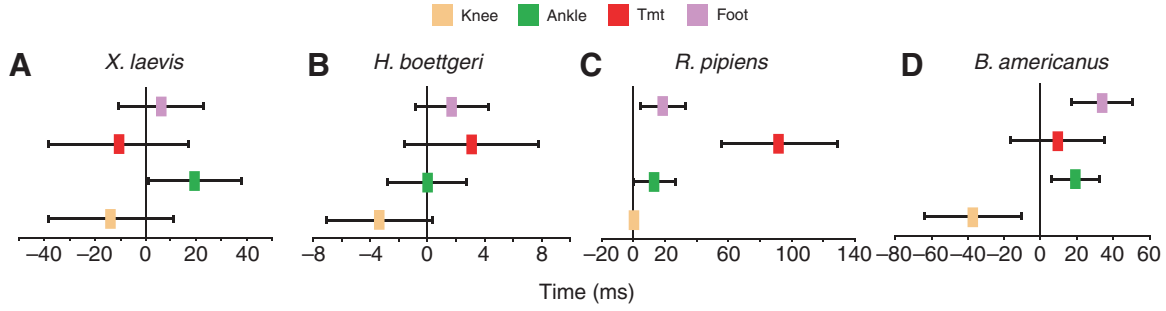

Fig. 2. Relative timing of joint extension. Onset of extension of the knee (orange), ankle (green), tmt (red) and foot (purple) with respect to the onset of hip extension (defined as 0 ms) in (A) *X. laevis* (*N*=39 trials among *N*=4 frogs), (B) *H. boettgeri* (*N*=48 trials among *N*=4 frogs), (C) *R. pipiens* (*N*=42 trials among *N*=4 frogs) and (D) *B. americanus* (*N*=52 trials among *N*=3 frogs). Negative values represent onset times prior to the onset of hip extension. Data are means ± s.d. pooled among trials for all individuals within each species.

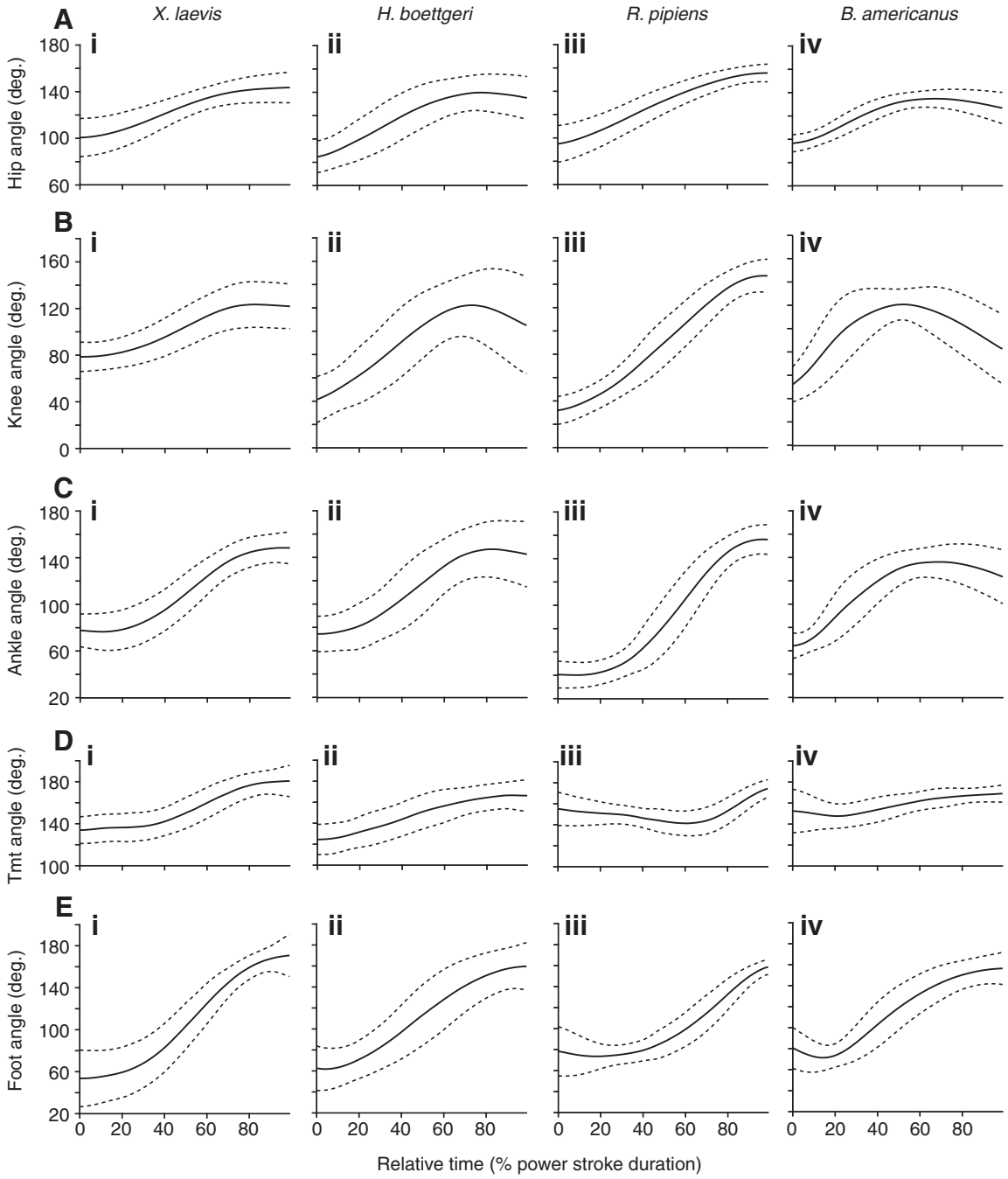

Fig. 3. Power stroke joint angle traces. (A) Hip angle, (B) knee angle, (C) ankle angle, (D) tmt angle and (E) foot angle traces for *X. laevis* (*N*=10 trials), *H. boettgeri* (*N*=15 trials), *R. pipiens* (*N*=20 trials) and *B. americanus* (*N*=19 trials; i–iv, respectively). Data are means (solid line) ± s.d. (broken line) for all trials within one representative individual within each species. The time axis has been normalized to the duration of the power stroke in all trials. Note that since these traces are drawn between the onset of center of mass (COM) acceleration and peak COM velocity, some joints have begun to extend earlier in the cycle.

were unique for each species. Mean minimum and maximum joint angles differed significantly for most comparisons between species (Table 2). Most notably, the mean minimum foot angle was highly variable among species, ranging from 54.2±8.1 to 79.3±21.8 to 83.4±10.4 to 103.9±15.6, in *X. laevis*, *H. boettgeri*, *R. pipiens* and *B. americanus*, respectively (mean ± s.e.m.; Table 2). Therefore, the range of foot rotation was highest in *X. laevis* and lowest in *B. americanus*. Despite species differences in joint angular excursions, mean joint extension patterns followed qualitatively similar sinusoidal increases in joint angle throughout the power stroke (Fig. 3). This general pattern was observed in all joints except the tmt joint in *R. pipiens* and *B. americanus*, which each showed minimal (<30 deg.) net joint extension (Fig. 3Diii,iv; Table 2). Most joint angles peaked near 100% of the power stroke duration; however, mean peak hip, knee and ankle angles in *B. americanus* were phase-shifted to 65%, 52% and 67% stroke duration, respectively (Fig. 3Aiv,Biv,Civ). For each multiple comparison in the current study, a two-way ANOVA was used to verify that

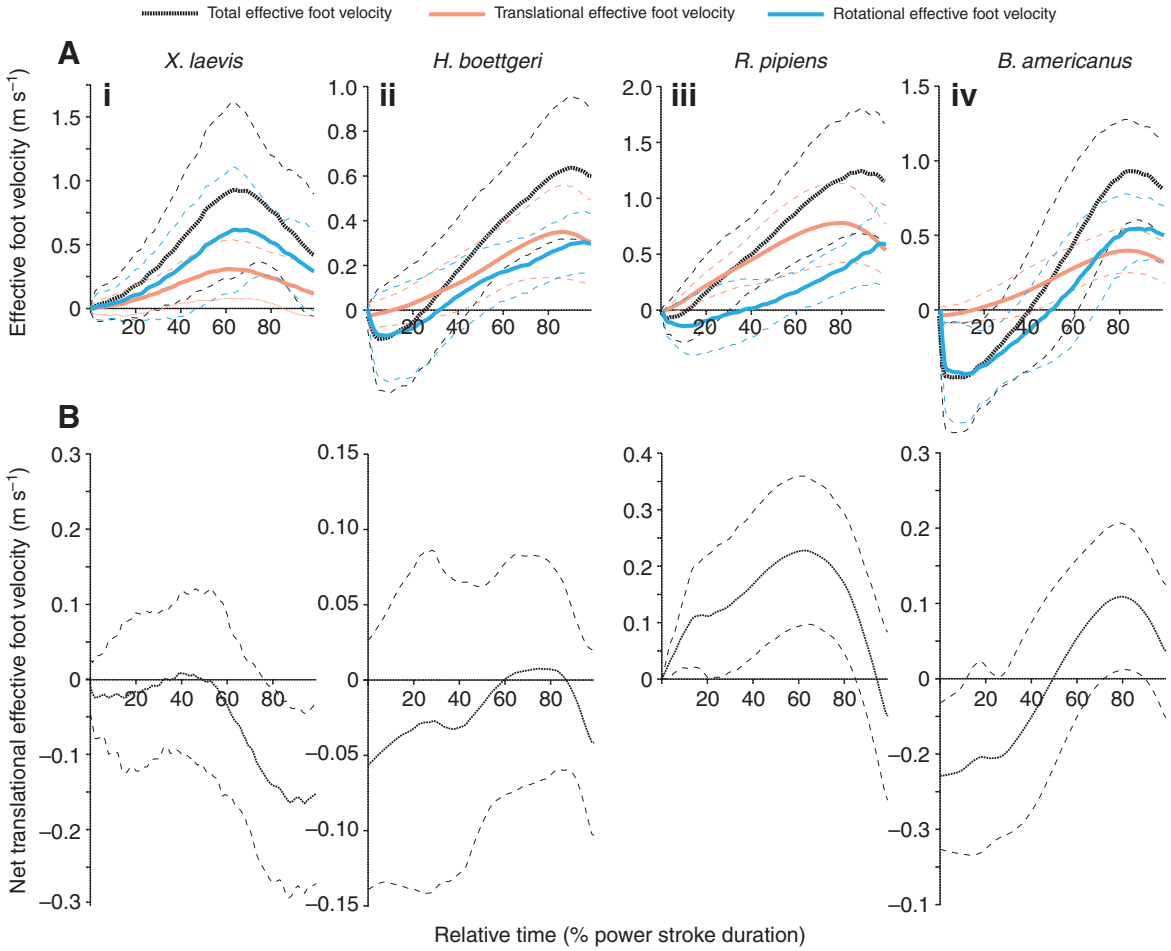

Fig. 4. Effective foot velocity traces. (A) Total effective foot velocity (black line), translational (red line) and rotational (blue line) components of effective foot velocity for *X. laevis* (*N*=39 trials among *N*=4 frogs), *H. boettgeri* (*N*=48 trials among *N*=4 frogs), *R. pipiens* (*N*=42 trials among *N*=4 frogs) and *B. americanus* (*N*=52 trials among *N*=3 frogs ; i–iv, respectively). (B) Net translational effective foot velocity (translational effective foot velocity – swimming velocity). Data are means (solid lines) ± s.d. (broken lines) for all trials pooled from all individuals within each species.

significant differences among species were not confounded by differences between individual frogs (P<0.05).

Effective foot velocity differences among species

As a consequence of variation in hind limb kinematics, *EFV* profiles were distinct among species. In each species, *EFV* increased during most of the power stroke (the period of positive COM, acceleration; Fig. 1B) and decreased late in the stroke (Fig. 4). Because *EFV* was still positive at the end of the power stroke, the COM began decelerating before full hind limb extension in all species (Fig. 4A). In *X. laevis*, peak *EFV* phase averaged 70±8% (Fig. 4Ai) with respect to the onset of the power stroke, which was significantly earlier compared with 88±3, 87±4 and 81±6% in *H. boettgeri*, *R. pipiens* and *B. americanus*, respectively (mean ± s.e.m.; ANOVA, Tukey–Kramer, P≤0.001 for all comparisons). The translational component of *EFV* in *X. laevis* peaked at 62±8% (Fig. 4Ai), which was significantly earlier than 83±8% in *H. boettgeri*, 78±2% in *R. pipiens* and 80±8% in *B. americanus*. Similarly, rotational *EFV* in *X. laevis* peaked significantly earlier in the power stroke, at 71±8% compared with

Table 3. Foot kinematics summary

	Peak *EFV* (m s^{-1})	Relative translational *EFV* (100% × peak *EFV*-t/peak *EFV*)	Relative rotational EFV (100% × peak EFV-r/peak EFV)	*P*-value (relative translational EFV *versus* relative rotational EFV)	Relative translational impulse (100% × translational impulse/max impulse)	Relative rotational impulse (100% × rotational impulse/max impulse)
X. laevis	1.17±0.16	32±5%	74±2%	<0.0001*	–2±8%	36±13%
H. boettgeri	0.73±0.15	55±3%	53±6%	0.98	15±10%	25±10%
R. pipiens	1.44±0.14	64±5%	51±7%	0.0004*	25±9%	13±6%
B. americanus	1.12±0.17	40±3%	62±2%	<0.0001*	20±16%	23±3%

Translational and rotational components of *EFV* are abbreviated *EFT*-t and *EFV*-r, respectively. All values are means ± s.e.m for *X. laevis* (*N*=39 trials among *N*=4 frogs), *H. boettgeri* (*N*=48 trials among *N*=4 frogs), *R. pipiens* (*N*=42 trials among *N*=4 frogs) and *B. americanus* (*N*=52 trials among *N*=3 frogs).
*Significant, paired t-test with α=0.05 adjusted by the sequential Bonferroni correction.

H. boettgeri, *R. pipiens* and *B. americanus* means of 88±2%, 92±5% and 82±5%, respectively. Magnitudes of relative translational *EFV* (100% peak translational *EFV*/peak total *EFV*) as well as relative rotational *EFV* were highly variable among species (Table 3). In *H. boettgeri*, there was no statistical difference between relative translational and rotational *EFV* (55±3% *versus* 53±6%; P=0.98). Relative rotational *EFV* was 74±2% in *X. laevis* and 62±2% in *B. americanus*, which was significantly higher than mean relative translational *EFV* of 32±5% and 40±3%, respectively (P<0.0001). However, in *R. pipiens* relative translational *EFV* was 64±5%, which was significantly higher than mean rotational *EFV* of 51±7% (P<0.0001;Table 3). In *H. boettgeri* and *B. americanus*, rotational *EFV* was negative early in the power stroke. This was likely due to slight asynchrony in the limbs for some swimming strokes of *H. boettgeri*. For *B. americanus*, however, a small burst of COM acceleration occurred late in the limb recovery phase, which is likely due to positive thrust caused by added mass effects (Nauwelaerts et al., 2005). Consequently, the COM began to accelerate slightly before (~80 ms) the onset of joint extension in most swimming strokes. Additionally, 'net translational *EFV*' (translational *EFV* – COM velocity) was calculated to obtain foot velocity in the global frame of reference. Strikingly, net *EFV* was almost entirely negative in *X. laevis* and *H. boettgeri* (peaking at ~0 m s^{-1}) compared with peak net *EFV* of 0.23±0.13 and 0.11±0.1 in *R. pipiens* and *B. americanus*, respectively (Fig. 4B).

Contributions of individual joint kinematics to total foot displacement

Throughout all recorded power strokes, total angular excursions at each leg joint contributed to the total translational displacement of the foot (Fig. 5A). In each species, the hip contributed most to total translational foot displacement. In *X. laevis*, the relative hip contribution to total translational displacement (100%×$\mathbf{d}_{t,hip}/\mathbf{d}_t$) was 61±6% compared with 8±6% and 31±5% for knee and ankle contributions, respectively. In *H. boettgeri*, *R. pipiens* and *B. americanus*, ankle extension contributed least to total translational displacement. Within each of the four species, all comparisons of group mean joint contributions to foot translation were significant (mean ± s.e.m.; ANOVA, Tukey–Kramer, P<0.003). However, the hip *versus* knee contributions to translational displacement were not significantly different in *B. americanus* (P=0.105).

Total rotational foot displacement was also a function of excursions at each limb joint (Fig. 5B). Each of the four species showed a similar pattern where the knee and tmt contributed least to the total change in foot angle. Most strikingly, the relative knee contribution to foot rotational displacement (100%×$\mathbf{d}_{r,knee}/\mathbf{d}_r$) was –75±14%, –256±67%, –170±38% and –138±18%, which decreased total foot angle change in *X. laevis*, *H. boettgeri*, *R. pipiens* and *B. americanus*, respectively. Since the knee angle is oriented opposite the other angles (i.e. the knee points laterally; Fig. 1A), knee extension reduces foot angle, causing negative knee contributions to peak angular displacement in all species. Notably, the tmt also contributed 61±17% and 75±22% to foot rotation in *X. laevis* and *H. boettgeri*, whereas in *R. pipiens* and *B. americanus* the tmt contributed negligibly (–32±24% and 8±30%, respectively) to total foot rotation. The relative contributions of the hip and ankle to foot rotation also varied among species. The hip contribution to foot rotation ranged from 52±21% to 64±11% to 90±23% to 160±37% in *B. americanus*, *X. laevis*, *R. pipiens* and *H. boettgeri*, respectively. Similarly, the ankle contribution to foot rotation ranged from 94±3% to 100±15% to 149±24% to 165±37% in *B. americanus*, *X. laevis*, *H. boettgeri* and *R. pipiens*, respectively. Within each species, differences among all joints were significant (ANOVA, Tukey–Kramer, P<0.012) except for hip *versus* tmt in *X. laevis* and hip *versus* ankle in *H. boettgeri* (Fig. 5B).

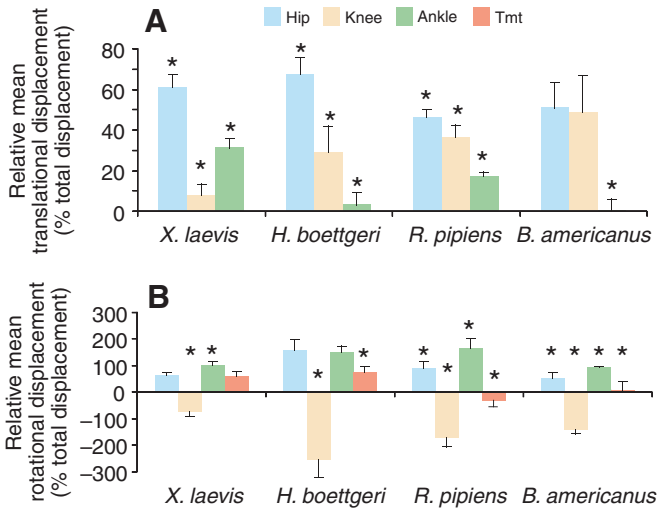

Fig. 5. Joint contributions to total translational and rotational foot displacement. (A) Bar graphs showing the relative contribution of the hip, knee and ankle to the total translational foot displacement over power strokes. Values are normalized to the total translational displacement of the foot. (B) Bar graphs showing the relative contribution of the hip, knee, ankle and tmt to the total rotational foot displacement over power strokes. Values are normalized to the total rotational displacement of the foot. Data are shown from *X. laevis* (N=39 trials among N=4 frogs), *H. boettgeri* (N=48 trials among N=4 frogs), *R. pipiens* (N=42 trials among N=4 frogs) and *B. americanus* (N=52 trials among N=3 frogs). Bars show group means ± s.e.m. for all trials pooled from all individuals within each species. *Significantly different (P<0.05) than group means for all other joints.

Contributions of individual joint kinematics to foot velocity

For all four species, joint extension at the hip, knee and ankle each contributed to foot translational velocity (Fig. 6). In *R. pipiens*, the relative hip contribution to translational velocity (100%×peak $\mathbf{v}_{t,hip}$/peak $\mathbf{v}_t$) was 43±5% (Fig. 6Aiii), which was significantly lower than 62±7%, 66±2% and 60±5% in *X. laevis*, *H. boettgeri* and *B. americanus*, respectively (mean ± s.e.m.; ANOVA, Tukey–Kramer, P<0.001 for all comparisons). The relative knee contribution to translational velocity varied considerably among species, with the highest mean of 56±19% in *B. americanus* (Fig. 6Biv) and lowest mean of 21±11% in *X. laevis* (Fig. 6Bi). Differences in the relative knee contribution to translational velocity were significant in both *X. laevis* and *B. americanus* compared with *H. boettgeri* and *R. pipiens* (P≤0.01). In all four species, ankle extension contributed less to translational velocity than hip extension. Mean contributions of ankle extension to translational velocity of 39±8%, 35±7% and 34±4% in *X. laevis*, *R. pipiens* and *B. americanus* (Fig. 5C), respectively, were statistically similar (P≥0.1), but significantly different from 26±6% in *H. boettgeri*.

Rotational foot velocity was also broken down into contributions from hip, knee, ankle and tmt joint extension (Fig. 7). The relative hip contribution to peak rotational velocity (100%×peak $\mathbf{v}_{r,hip}$/peak $\mathbf{v}_r$) was 49±11% in *R. pipiens* (Fig. 7Aiii), which was statistically similar to 50±10% in *B. americanus* (Fig. 7Aiv; P=0.62). Mean contribution of hip extension was 70±5% in *H. boettgeri* and 34±3% in *X. laevis*, each differing significantly from *R. pipiens* and *B. americanus* (P≤0.001). In *X.*

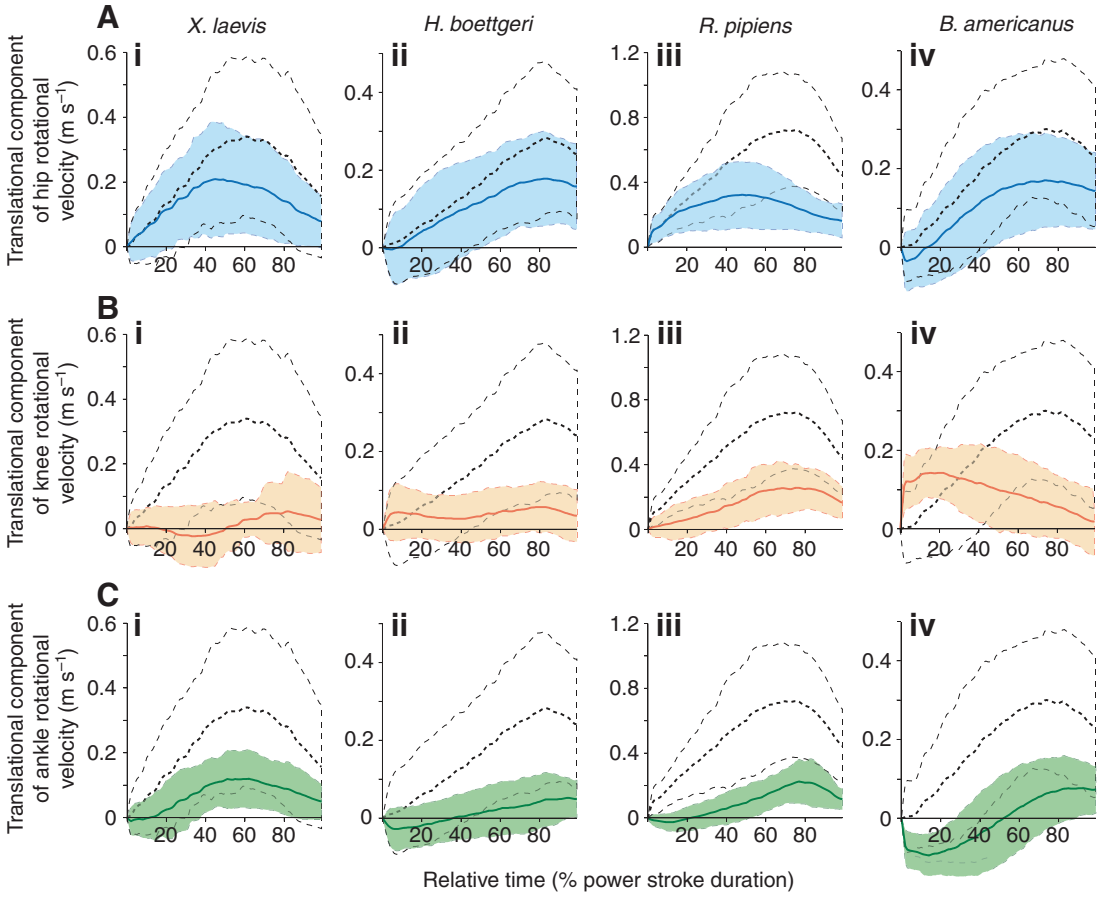

Fig. 6. Joint extension velocity contributions to foot translational velocity. Traces of contributions from (A) hip (blue), (B) knee (orange) and (C) ankle (green) to foot translational velocity (black) for *X. laevis* (*N*=39 trials among *N*=4 frogs), *H. boettgeri* (*N*=48 trials among *N*=4 frogs), *R. pipiens* (*N*=42 trials among *N*=4 frogs) and *B. americanus* (*N*=52 trials among *N*=3 frogs; i–iv, respectively). Data are means (solid lines) ± s.d. (broken lines and shaded areas) for all trials pooled from all individuals within each species.

laevis, the mean knee contribution to peak rotational velocity, –49±11% (Fig. 7Bi), was significantly higher ($P \leq 0.001$) than –125±16%, –106±14% and –120±10% in *H. boettgeri*, *R. pipiens* and *B. americanus*, respectively, which did not differ significantly ($P > 0.7$). Mean contributions of ankle extension to peak rotational velocity were 70±4% in *X. laevis*, 111±29% in *H. boettgeri*, 156±10% in *R. pipiens* and 118±10% in *B. americanus*. Differences among all mean ankle contributions were statistically significant ($P \leq 0.001$) except for the difference between *H. boettgeri* and *B. americanus* (P=0.89). For each species, the ankle showed the highest relative contribution to peak rotational velocity compared with hip, knee and tmt joints. The relative tmt contribution to peak rotational velocity averaged –15±24% in *R. pipiens* (Fig. 7Diii), which was statistically similar to –1±47% in *B. americanus* (Fig. 7Div; P=0.97). Mean peak tmt extension contributed 57±20% to peak rotational velocity in *X. laevis* and 51±30% in *H. boettgeri*, each significantly higher than *R. pipiens* and *B. americanus* ($P \leq 0.001$).

Estimated thrust from foot translation and rotation

Net hydrodynamic thrust impulse (i.e. the time integral of estimated hydrodynamic thrust) in *H. boettgeri*, *R. pipiens* and *B. americanus* was produced both by translational and rotational foot motion (Fig. 8A; Table 3). By contrast, net thrust impulse was only derived from rotational foot motion in *X. laevis*. For data pooled across all swimming speeds, the mean relative translational impulse (100% × translational impulse/maximum impulse) was 15±10%, 25±9% and 20±16% in *H. boettgeri*, *R. pipiens* and *B. americanus*, respectively, but only –2±9% in *X. laevis*. The mean relative rotational impulse was 36±13%, 25±10%, 13±6% and 23±3% in *X. laevis*, *H. boettgeri*, *R. pipiens* and *B. americanus*. Paired *t*-tests within each species revealed that relative translational and rotational impulses were significantly different in *X. laevis*, *H. boettgeri* and *R. pipiens* ($P < 0.0001$) but statistically similar in *B. americanus* (P=0.64). Inter-specific differences in translational *versus* rotational thrust impulses were nearly independent of swimming speed. For slow swimming trials (<30% peak swimming velocity), mean relative translational *versus* rotational impulses were –1±3% *versus* 18±7%, 0.4±6% *versus* 17±15% and 10±5% *versus* 5±3% for *X. laevis*, *H. boettgeri* and *R. pipiens*, respectively (Fig. 8B). Similarly, relative translational *versus* rotational impulses for fast swimming trials (>60% peak swimming velocity) were –5±18% *versus* 61±30%, 24±14% *versus* 33±12% and 33±13% *versus* 19±9% for *X. laevis*, *H. boettgeri* and *R. pipiens* (Fig. 8C). Only pooled data were analyzed for *B. americanus* because most of the swimming trials were within 60% of maximum swimming speed.

Peak velocity for swimming strokes positively correlated with thrust impulse in all four species observed (Table 4). *X. laevis*, *H. boettgeri* and *R. pipiens* showed the strongest correlation between peak velocity and thrust impulse, compared with the relatively weak relationships observed in *B. americanus* frogs (Table 4).

DISCUSSION

Comparing hind limb kinematics among frog species

The present study aimed to quantify hind limb kinematics patterns and estimate the hydrodynamic forces produced by the feet in four anuran species. Based on prior studies (Peters et al., 1996; Johansson and Lauder, 2004; Nauwelaerts et al., 2005), I expected that semi-

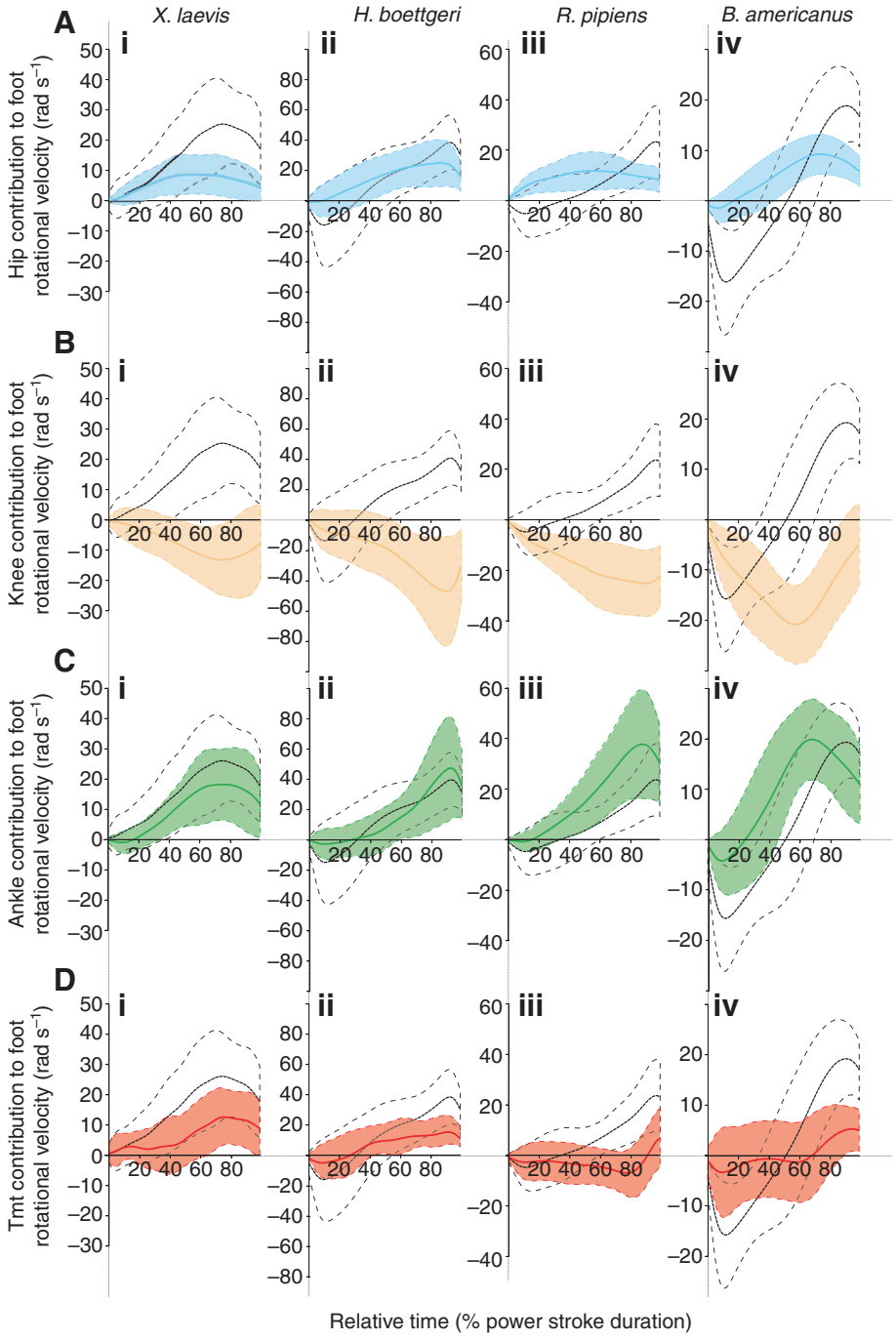

Fig. 7. Joint extension velocity contributions to rotational velocity. Traces of contributions from (A) hip (blue), (B) knee (orange), (C) ankle (green) and (D) tmt (red) to foot rotational velocity (black) for *X. laevis* (*N*=39 trials among *N*=4 frogs), *H. boettgeri* (*N*=48 trials among *N*=4 frogs), *R. pipiens* (*N*=42 trials among *N*=4 frogs) and *B. americanus* (*N*=52 trials among *N*=3 frogs; i–iv, respectively). Data are means (solid lines) ± s.d. (broken lines and shaded areas) for all trials pooled from all individuals within each species.

aquatic/terrestrial species (represented by *B. americanus* and *R. pipiens*) would primarily use proximal leg joints to produce translational foot motion to power swimming. By contrast, purely aquatic frogs (represented by *X. laevis* and *H. boettgeri*) were expected to swim by rotating their feet *via* distal joint extension (Richards, 2008). Findings from the current study do not fully support either hypothesis. As expected, thrust produced by foot rotation is significantly higher than translational-based thrust in the two aquatic species *X. laevis* and *H. boettgeri*. However, leg and foot kinematics are not consistent within aquatic or semi-aquatic/terrestrial groups, despite similar maximum swimming performance among them. Instead, the four species examined represent a continuum between propulsion driven exclusively by rotational motion (*X. laevis*), mostly rotational motion (*H. boettgeri*), rotational and translational motion (*B. americanus*), and mostly translational motion (*R. pipiens*).

In all four species, frogs increased swimming speed from one stroke to the next by increasing the thrust impulse produced at the feet (Table 4). However, the differential use of translational *versus* rotational components of thrust varies among these species (Fig. 8). Moreover, inter-specific differences in thrust mechanism do not differ significantly between slow and fast swimming speeds (Fig. 8B,C). The mechanism by which *B. americanus* modulates swimming speed remains unclear, given that swimming speed is only weakly correlated with thrust impulse in most of the frogs observed (Table 4). Perhaps the weak correlation is explained by a

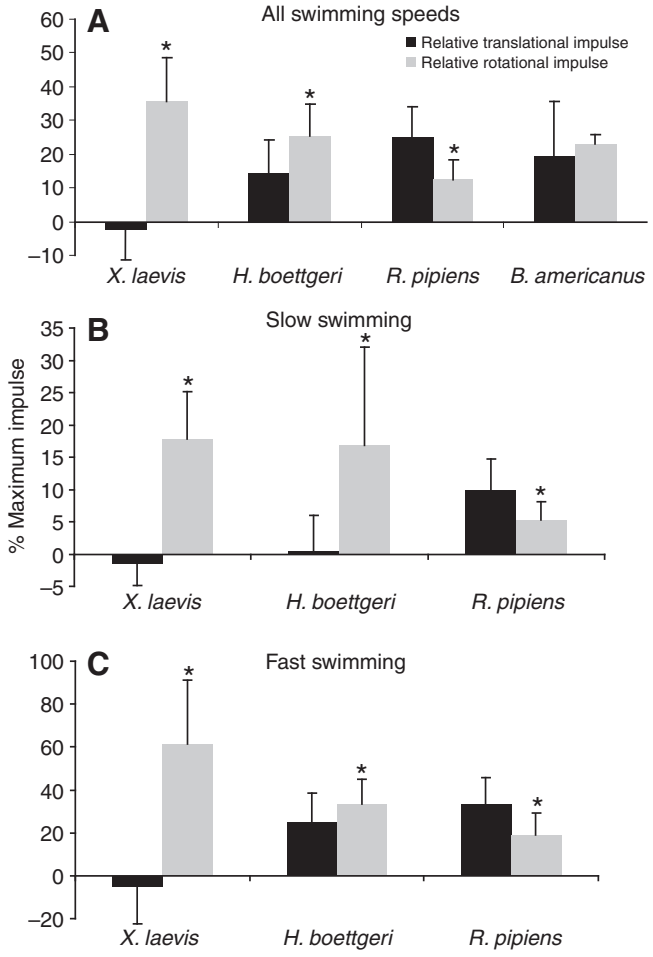

Fig. 8. Thrust impulse produced by foot translation and rotation. Black bars represent relative translational impulse (100% × translational impulse/maximum thrust impulse), and gray bars represent relative rotational impulse (100% × rotational impulse/maximum thrust impulse). Maximum impulse is the highest recorded impulse among all individuals within each species. Bars are means ± s.e.m. Data are from (A) trials pooled across all swimming speeds, (B) slow swimming trials only (<30% maximum swimming velocity) and (C) fast swimming trials only (>60% maximum swimming velocity). Note that *B. americanus* is excluded from B and C because the observed range of swimming velocities was too narrow (see text). *Significantly different (P<0.05), paired t-tests.

very narrow range of swimming speeds in *B. americanus* compared with the other three species. Additional peculiarities observed in *B. americanus* swimming are discussed in further detail below.

General kinematic patterns of the joints and feet during swimming

Body kinematics patterns are superficially similar among all four species. Frogs swim by a 'kick-and-glide' mechanism, causing rapid acceleration of the COM followed by a glide phase in which the COM velocity gradually decreases due to the drag on the body and the limbs. After the glide, the leg joints flex to retract the limb in preparation for the subsequent stroke (Fig. 1B). During the recovery phase, the COM velocity decreases sharply. The glide and recovery strokes are highly variable within individuals (Nauwelaerts et al., 2001). Moreover, the length of the glide phase, relative to the propulsive phase, varies among the species observed (discussed in further detail below). Therefore, only the power stroke portion is analyzed in the current study to avoid the confounding variation in glide and recovery strokes among species.

All species observed employ a similar power stroke pattern driven by temporally staggered extension of the leg joints (Fig. 2), resulting in cranio-caudal foot translation and rotation. Despite temporally staggered onsets of joint extension in all species, the hip, knee and ankle generate translational velocity of the feet (Fig. 6A–C). Similarly, the hip and ankle contribute rotational velocity to the feet in all species (Fig. 7A,C). Importantly, because the knee angle faces medially (unlike all other joints, which face laterally), knee extension velocity is negative with respect to the other joints. For example, on the left leg, hip, ankle, and tmt extend in the anticlockwise direction whereas knee extension is clockwise (Fig. 1A). Therefore, as a consequence of the conserved limb morphology among anurans, knee extension contributes negatively to foot rotational velocity in all four species (Fig. 7B).

Due to coordinated joint extension, all species achieve net positive *EFV* during power strokes (Fig. 4A). Since *EFV* is both a function of foot velocity and the foot's projected area in flow, it is a useful measure of how translational and rotational foot velocity interact to generate drag-based thrust (drag-based thrust $\propto EFV^2$). In all species tested, *EFV* peaks prior to maximum COM velocity. Consistent with observations in *R. pipiens* (Johansson and Lauder, 2004) and *H. boettgeri* (Gal and Blake, 1988), the leg joints continue to extend after the end of the power stroke (i.e. after the period of positive COM acceleration). The duration of the limb extension phase (the period between the beginning of the power stroke and the point where *EFV* reaches zero; Fig. 1B) is roughly twice the duration of the power stroke, which does not significantly differ among species (P>0.05). Consequently, in frogs, only approximately the first half of limb extension duration provides enough thrust at the feet to overcome hydrodynamic drag and added mass on the body. The remaining portion of limb extension serves to straighten the leg to reduce drag on the animal's profile (Peters et al., 1996), as well as to assist shedding of the attached vortices on the foot (Johansson and Lauder, 2004) to minimize retarding added-mass-based force (see Daniel, 1984).

Species differences in the mechanism for producing thrust

All four frog species shared superficial similarities in body and limb morphology (Table 1), joint angle patterns (Fig. 3) and foot velocity patterns (Fig. 4). Despite these similarities, hydrodynamic modeling suggests dramatic differences in the propulsion mechanics of these species. A recently developed forward-inverse dynamics approach (Richards, 2008) allows the estimation of total thrust as the sum of thrust produced by translational and rotational foot motion. In *X. laevis* and *H. boettgeri*, most of the thrust required for swimming comes from rotational foot motion whereas *R. pipiens* generate thrust mainly by foot translation (Fig. 8). Thrust estimates from *B. americanus*, however, were highly variable and, consequently, the hydrodynamic mechanism in toads is unclear from the current study and will be discussed below.

Although *EFV* traces are useful for relating joint extension to resultant foot motion in a local coordinate system, predicting species-specific thrust patterns also requires consideration of foot motion in the global frame of reference. After Gal and Blake (Gal and Blake, 1988), translational *EFV* was converted to 'net translational *EFV*' (translational *EFV* – COM velocity) to approximate foot velocity relative to the background flow surrounding the foot as the body moves forward. For example, if translational *EFV*=COM velocity, the feet are pushing backward

Table 4. Linear regression results: peak velocity *versus* estimated thrust impulse

Species	Individual	*N* (swimming strokes)	Swimming velocity range (min to max m s^{-1})	Thrust impulse range (N ms)	Thrust impulse/ body mass range (N ms kg^{-1} body mass)	R^2	*P*-value
X. laevis	Frog 1	11	0.165–1.299	4.375–28.658	0.156–1.023	0.987	<0.0001*
X. laevis	Frog 2	10	0.293–1.301	3.909–22.294	0.138–0.788	0.735	0.001*
X. laevis	Frog 3	9	0.189–1.145	4.034–40.229	0.155–1.55	0.948	<0.0001*
X. laevis	Frog 4	9	0.152–0.975	3.778–23.267	0.189–1.163	0.753	0.001*
H. boettgeri	Frog 1	14	0.201–0.594	0.060–0.466	0.037–0.282	0.742	<0.0001*
H. boettgeri	Frog 2	6	0.141–0.708	0.056–0.369	0.059–0.390	0.72	0.02*
H. boettgeri	Frog 3	11	0.233–0.717	0.168–0.560	0.146–0.487	0.297	0.048*
H. boettgeri	Frog 4	17	0.109–0.767	0.049–0.561	0.046–0.535	0.738	<0.0001*
R. pipiens	Frog 1	4	0.457–1.250	7.732–27.423	0.258–0.914	0.595	0.145
R. pipiens	Frog 2	11	0.331–1.883	7.433–43.409	0.186–1.085	0.645	0.002*
R. pipiens	Frog 3	7	0.398–1.328	6.247–36.192	0.156–0.905	0.926	<0.0001*
R. pipiens	Frog 4	20	0.303–1.363	0.924–15.900	0.056–0.964	0.87	<0.0001*
B. americanus	Frog 1	8	0.155–0.493	0.555–5.410	0.056–0.546	0.779	0.002*
B. americanus	Frog 2	19	0.278–0.457	0.996–6.294	0.023–0.144	0.004	0.808
B. americanus	Frog 3	25	0.221–0.432	0.489–5.016	0.011–0.112	0.365	0.001*

*Significant *P*-value (α<0.05).

against the water at the same rate that the COM progresses forward. Therefore, no translational thrust is produced because the tmt joint (i.e. the base of the foot) is stationary in the global reference frame. Importantly, when net translational *EFV*=0, rotational *EFV* generates enough thrust to overcome drag and added mass on the body, enabling the COM to move forward. Foot translational velocity in *X. laevis* and *H. boettgeri* seldom exceeds the forward COM velocity. Consequently, net translational *EFV* is negative throughout most swimming strokes (Fig. 4B). In the latter half of the power stroke, *R. pipiens* and *B. americanus* show the opposite pattern of rapid translational velocity and relatively slower forward COM velocity due to the backward 'slip' of the foot.

The individual roles of hind limb joints in propulsion

Combining the above hydrodynamic modeling with joint kinematics measurements enables a detailed analysis of how individual joints contribute to propulsion. In all four species examined, hip extension contributes largely to both foot translation and rotation (Fig. 5). In *R. pipiens*, the hip generates propulsive motion primarily by translating the foot. However, because net translational *EFV* is low in *X. laevis* and *H. boettgeri*, the hip contributes directly to propulsion only by helping to rotate the foot. Although the knee diminishes rotational velocity (therefore likely reducing rotational thrust) in all four species, the translational component of knee extension contributes to thrust most strongly in *R. pipiens*, but also in *H. boettgeri* and *B. americanus*. The roles of the ankle and tmt joints are highly variable among species. *X. laevis* and *R. pipiens* use ankle extension both to translate and rotate the feet. However, the ankle of *X. laevis* likely contributes to propulsion by assisting foot rotation whereas *R. pipiens* likely uses the ankle to produce translational thrust (helping to maintain the foot at ~90 deg. to flow). By contrast, the ankle does not contribute to translational velocity in *H. boettgeri* and *B. americanus* but likely contributes substantially to thrust by rotating the foot.

The varied use of individual leg joints among species suggests that different species employ unique joint coordination strategies to power swimming. Variation in the underlying joint kinematics can be understood in the context of hydrodynamic differences among species. For example, *R. pipiens* frogs effectively generate translational thrust by maintaining ~90 deg. foot angle in flow for the first approximately half of the power stroke (Peters et al., 1996; Nauwelaerts et al., 2005; present study; Fig. 3Eiii), maximizing the foot area projected into flow. Pure translation (i.e. no net change in foot angle) requires three aspects of coordination. Firstly, hip and knee extension must be synchronized to cause the foot to move mainly in the cranio-caudal axis (see supplementary material, Movie 2 *versus* Movie 3). If the knee were to extend further (or earlier) than the hip, the feet would move laterally instead of caudally (Movie 4 in supplementary material). Additionally, if the hip were to extend further (or earlier) than the knee, the foot would rotate instead of translate. *R. pipiens*, unlike the three other species observed, extend the hip and knee synchronously (Fig. 2), enabling the transfer of joint rotation to foot translation. Secondly, extension velocities of the knee and ankle should be similar. This allows foot rotation caused by the ankle to cancel foot counter-rotation caused by knee extension, enabling cranio-caudal foot translation at a fixed foot angle (Movie 5 in supplementary material). Lastly, hip extension (important for foot translation) also causes foot rotation. Hip-generated foot rotation is likely balanced by negative rotation (i.e. flexion) at the tmt joint in the first approximately half of the stroke (Fig. 3Diii), possibly explaining why *R. pipiens* is the only species observed to generate negative net rotational motion at the tmt joint (Fig. 5B; Fig. 7Diii). Speculation on the functional significance of the 'translational' swimming stroke in ranid frogs is discussed below.

Instead of minimizing foot rotation (as seen in *R. pipiens*), *X. laevis* appear to coordinate limb joints to enhance rotational foot velocity. As noted above, knee extension (synchronized with hip extension) produces positive foot translational velocity at the expense of foot rotational velocity. This tradeoff suggests that increased extension of distal joints (ankle and tmt) may compensate for counter-rotation at the knee to produce the necessary foot rotation. In *H. boettgeri*, *R. pipiens* and *B. americanus*, the knee is the second most important joint contributing to translational foot motion. Interestingly, in *X. laevis*, the mean knee angle range is ~50 deg. compared with ~100 deg. in all other species tested (Fig. 3; Table 2). Because *X. laevis* rely heavily on rotational foot velocity for thrust (Fig. 8), knee extension may be kept minimal to reduce foot counter-rotation. *X. laevis*, however, require a small amount of translational thrust to accelerate the COM early in the stroke (Richards, 2008) and therefore must produce the necessary foot translation by substantial ankle rotation (to compensate for reduced knee extension). Similarly, *B. americanus* kinematics also reveal

strategies to enhance foot rotation. In *B. marinus*, the knee is the first joint to extend, pushing the feet laterally early in the stroke (Gillis and Biewener, 2000). Later in the stroke, the ankle and hip extend to rotate the foot. If the hip and ankle were in phase with the knee, extension at the knee would cancel foot rotation from hip and ankle extension (see supplementary material, Movie 5 *versus* Movie 6). Importantly, however, rapid swimming likely requires all joints to extend in phase to maximize both translational and rotational based thrust (Richards, 2008). Consequently, the out-of-phase coordination of *B. americanus* joints may partially explain their relatively slow maximum swimming speed (~7 BL s^{-1} compared with >20 BL s^{-1} in the three other species tested).

Limitations of blade element modeling for estimating thrust in frogs

The blade element model used for the current study has been verified previously (Richards, 2008); however, limitations arise using this approach. All hydrodynamic calculations in the current study assume that the feet are the principal propulsive surfaces on the hind limbs. This assumption is valid for *X. laevis*, *H. boettgeri* and *R. pipiens*, which each have large ratios of foot area:frontal body area (0.56±0.09, 0.42±0.02 and 0.15±0.07, respectively; mean ± s.d.) compared with *B. americanus* (0.08±0.05). This suggests that *B. americanus* feet are less effective at producing thrust for any given stroke pattern. Toads may rely on thrust produced by their leg segments in addition to the foot, possibly explaining why thrust impulse from the feet is a poor predictor of swimming performance. Future modifications to the blade element model could include hydrodynamic reaction forces from the upper and lower leg to account for all possible propulsive surfaces. An additional limitation is that the feet are approximated as flat plates with constant area. However, the feet change their shape and area throughout the course of a swimming stroke (C.R., personal observations), implying that animals may benefit by controlling their propulsor flexibility (Lauder et al., 2006). This problem could be addressed by a 3-D analysis of foot kinematics coupled with more advanced modeling tools (e.g. computational fluid dynamics) as well as robotic models (Lauder et al., 2007) to determine how dynamic propulsor shape influences hydrodynamic performance in frogs.

In addition to the limitations of the blade element model, there are three important species differences not accounted for by the analytical approaches used in the current study. Firstly, *R. pipiens* and *B. americanus* most often swim at the surface, whereas *X. laevis* and *H. boettgeri* swim fully submerged. Frogs swimming at the surface potentially incur additional drag on the body due to bow wave formation. The importance of drag due to wave formation can be assessed from the Froude number [*Fr*=swimming velocity/(gravitational acceleration × outstretched length of the frog)$^{0.5}$ (Hoerner, 1965; Johansson and Lauder, 2004). Such surface drag effects are substantial at approximately $0.4<Fr<0.8$ (Hoerner, 1965; Johansson and Lauder, 2004). *B. americanus* frogs swim slowly (maximum *Fr*~0.4), suggesting that surface wave drag is negligible. During rapid swimming (*Fr*>~0.8), *R. pipiens* advance forward faster than the time required for a bow wave to develop (Johansson and Lauder, 2004). At intermediate speeds (*Fr*~0.5), formation of bow waves likely causes the current model to underestimate body drag. However, increasing the body coefficient of drag by up to 4-fold in the hydrodynamic model did not significantly affect calculations of translational *versus* rotational components thrust. Therefore, behavioral differences of surface *versus* submerged swimming are not likely to account for the species differences in hydrodynamic mechanism reported in the current study. Secondly, *X. laevis* and *H. boettgeri* move their legs in the horizontal plane during normal, level swimming (C.R., personal observations). However, ranid frogs extend their legs slightly downwards in addition to the backward propulsive motion (Johansson and Lauder, 2004; Nauwelaerts et al., 2005), resulting in a downward-directed vortex ring and an upward force on the frog body (Johansson and Lauder, 2004). Since all of the calculations in the current study are from joint angles projected onto the horizontal plane, the analytical approach used here does not account for the downward motion of the legs. However, the slight (~14 deg.) angle of the frog body relative to horizontal [see fig. 2 in Johansson and Lauder (Johansson and Lauder, 2004)] would cause only a slight underestimate (~4%) of translational foot displacements, which is unlikely to bias the calculations used in the current study. Thirdly, the four species observed show drastic differences in the length of the glide phase relative to the propulsive phase. *X. laevis* and *H. boettgeri* individuals often (~30–50% of trials) truncate the glide phase whereas *R. pipiens* usually (~80% of trials) extend the glide phase until swimming velocity has reached zero. *B. americanus*, however, moves the legs continuously without gliding. The functional significance of such glide length differences is unclear. Perhaps glide length is correlated with the propulsive strategy used. For example, the extended glide phase (as seen in *R. pipiens*) may be a gliding strategy that is used for translational-driven strokes, whereas the shortened glide phase may be associated with rotational-driven strokes. Future modeling that accounts for the hydrodynamics of propulsive, glide and recovery stroke phases could be used to determine how propulsion and glide strategies can be coupled to enhance swimming performance (e.g. mean speed and efficiency over several swimming strokes).

Species diversity of kinematic and hydrodynamic patterns: functional and evolutionary considerations

Variation in kinematics and estimated hydrodynamics among species is potentially explained by three effects. Firstly, shared similarities between aquatic frogs (e.g. foot rotation-powered swimming in *X. laevis* and *H. boettgeri*) may reflect specializations for swimming. Despite similarities in morphology (Table 1) and performance among the ranid and pipid species observed, differences in hind limb kinematics and hydrodynamics suggest underlying differences in joint mechanics (e.g. muscle work, joint work, mechanical efficiency). Recent hydrodynamic modeling of swimming frogs proposed that mechanical efficiency (work done on the COM/net work done at the joints) is highly dependent on foot kinematics. At any given swimming speed, the most efficient swimming strokes are predicted to require a high ratio of foot rotational velocity to translational velocity [i.e. peak efficiency is predicted at a rotational to translational velocity ratio of ~1.7:1 (Richards, 2008)]. Perhaps obligatorily aquatic frogs (represented by *X. laevis* and *H. boettgeri*) rely heavily on rotational foot motion to increase swimming efficiency. Future studies could apply inverse dynamics to model mechanical power and work produced at the leg joints to estimate if mechanical efficiency is higher in aquatic *versus* semi-terrestrial and terrestrial frogs.

Secondly, characteristics of *X. laevis* and *H. boettgeri* may represent an ancestral (generalized) propulsive strategy in anurans that has become modified in more derived species that excel in jumping. This hypothesis is supported by the fact that, as pipid frogs, *X. laevis* and *H. boettgeri* are basal to the neobatrachia, which comprise most other frog species (Tree of Life; http://tolweb.org/Anura/16963). The more highly derived Ranidae and Bufonidae (belonging to neobatrachia) are much stronger

jumpers than *X. laevis* or *H. boettgeri* (C.R., personal observations). Although jumping evolved very early in anurans (Shubin and Jenkins, 1995; Jenkins and Shubin, 1998), jumping ability is highly variable among species (Rand, 1952; Jug, 1978). Among the species in the current study, *R. pipiens* is the strongest jumper, reaching maximum jump distances (relative to body mass) ~1.7 fold higher than in *B. americanus* (Emerson, 1977). *R. pipiens* also shows the most extreme dependence on foot translational velocity during swimming. Recent work on *R. esculenta* predicted that a high moment of inertia of the feet (relative to other leg segments) would benefit swimming by helping to maintain the foot at 90 deg. to flow by minimizing foot rotation (Nauwelaerts et al., 2007). Counter to their predictions, these workers found a positive correlation between performance and foot moment of inertia in jumping, but not in swimming. During jumping, increased foot moment of inertia may help to stabilize the feet as the proximal joints extend, maximizing the period of ground contact. If this is true, the translational-driven swimming seen in ranids (and possibly other powerful jumpers) may simply be a consequence of each foot's inertial resistance to rotation. A future analysis could include *Arcis crepitans*, a semi-aquatic hylid frog that is capable of jumps ~2–3× further than *R. pipiens* (Rand, 1952; Zug, 1978). Analysis of leg segment masses and moments of inertia among aquatic and semi-aquatic species might also help explain variation in swimming mechanics among frogs.

Thirdly, variation among species may correlate with phylogenetic differences rather than functional differences between purely aquatic and semi-terrestrial species. My findings demonstrate that foot-rotation-powered swimming only appears in the two aquatic species observed here. However, these findings cannot resolve whether 'foot rotational' swimming is a specialization for the aquatic habitat or, rather, is a shared trait among aquatic pipid species. Future studies on additional pipid, as well as neobatrachian taxa, could apply similar kinematics methods as employed here to achieve a wider sample of hind limb function. Independent contrasts analysis could then be used to establish if functional differences among species correlate with habitat (aquatic, semi-aquatic, terrestrial, arboreal) or with phylogenetic distance (Felsenstein, 1985).

Data from the current study demonstrate striking functional differences between anuran species during swimming. Within the study of frog swimming, these findings shed new light both on earlier important work (e.g. Gal and Blake, 1988; Peters et al., 1996), as well as more recent investigations. For example, Gal and Blake proposed a novel propulsion mechanism in *H. boettgeri* whereby the right and left feet produce a central backward jet as they approach the midline (Gal and Blake, 1988). Recent work in ranid frogs using digital particle image velocimetry (DPIV) (Johansson and Lauder, 2004; Nauwelaerts et al., 2005) shows no evidence for a central jet. However, findings from the current study show highly divergent kinematics and hydrodynamics between *H. boettgeri* and *R. pipiens*. A new study using DPIV in *Hymenochirus* would be required to reevaluate Gal and Blake's original claim.

Summary: predicting foot hydrodynamic function from joint kinematics

The current study offers simple analytical tools for integrating joint kinematics and hydrodynamics in a multi-joint limb. Given the apparent complexity of limb motion by multiple joints, one is tempted to only present descriptions of the joint extension patterns in the absence of any functional interpretation. I propose that resolving limb kinematics into translational *versus* rotational *EFV* is useful for presenting limb kinematics in a functional context. Moreover, the relative contributions of individual joints to propulsion are reasonably well predicted by analyzing joint contributions to translational and rotational velocity. In the current study, positive net translational *EFV* (e.g. *R. pipiens*) results from the feet translating backward faster than the animal advances forward. This suggests that the observed hip, knee and ankle extension, with minimized tmt extension, produces thrust from translational foot velocity. Conversely, negative net translational *EFV* (e.g. *X. laevis* and *H. boettgeri*) results from the body moving forward faster than the feet translate backward. This suggests an alternative mechanism for producing thrust; the observed rapid extension of the hip, ankle and tmt, with minimized knee extension, produces thrust from rotational velocity. As confirmed by hydrodynamic modeling, the kinematic observations suggest that pipids swim mainly by rotation-driven thrust whereas ranids swim mainly by translation-driven thrust.

Conclusions

Despite assumptions of prior literature, kinematics of swimming anurans are highly species specific, even among aquatic and semi-aquatic/terrestrial groups. Although time-varying patterns of joint kinematics appear superficially similar, differences in the magnitude and timing of joint velocity accumulate from proximal to distal. This results in dramatic differences in effective foot velocity when comparing patterns among species. Consequently, the hydrodynamic function of anuran feet varies from producing mainly translational thrust (unique to ranid frogs) to producing mainly rotational thrust (unique to pipid frogs). The current study, therefore, motivates future studies in which a broader sample of anuran diversity can be compared by the simple kinematic analyses presented here. Such a study would further illuminate how frog morphological diversity (both at the level of the musculoskeletal system and the whole body) affects the kinematics and hydrodynamics used to power swimming.

LIST OF SYMBOLS AND ABBREVIATIONS

BL	body lengths
COM	center of mass
$\mathbf{d}_r$	angular displacement
$\mathbf{d}_t$	translational displacement
EFV	effective foot velocity
L_f	foot length
L_{fem}	femur length
L_{tars}	proximal tarsal length
L_{tib}	tibia–fibula length
tmt	tarsometatarsal
$\mathbf{v}_l$	lateral translational velocity
$\mathbf{v}_r$	rotational velocity
$\mathbf{v}_t$	translational velocity
θ_{ankle}	ankle angle
θ_f	foot angle
θ_{hip}	hip angle
θ_{knee}	knee angle
θ_{tmt}	tarsometatarsal angle

ACKNOWLEDGEMENTS

I thank Pedro Ramirez for animal care and I greatly thank my PhD advisor, Andrew Biewener, for invaluable advice and mentorship in addition to the lab space and equipment necessary for this work. I thank Tim Higham for statistics advice and Brian Joo for assistance with data collection. I also thank members of my thesis committee: George Lauder, Farish Jenkins, Jr, Jack Dennerlein and Anna Ahn for helpful comments on this work. I am thankful for helpful comments on the preparation of this manuscript provided by Andrew Biewener, Em Standen, Carolyn Eng and anonymous reviewers. This work was funded by the National Science Foundation's Integrative Graduate Education and Research Traineeship (IGERT) program, the Chapman Fellowship and the Department of Organismic and Evolutionary Biology at Harvard.

REFERENCES

Daniel, T. L. (1984). Unsteady aspects of aquatic locomotion. *Am. Zool.* **24**, 121-134.

Emerson, S. B. (1978). Allometry and Jumping in frogs: helping the twain to meet. *Evolution* **32**, 551-564.

Felsenstein, J. (1985). Phylogenies and the comparative method. *Am. Nat.* **125**, 1-15.

Gal, J. M. and Blake, R. W. (1988). Biomechanics of frog swimming: II. Mechanics of the limb-beat cycle in Hymenochirus Boettgeri. *J. Exp. Biol.* **138**, 413-429.

Gillis, G. B. and Biewener, A. A. (2000). Hindlimb extensor muscle function during jumping and swimming in the toad (*Bufo marinus*). *J. Exp. Biol.* **203**, 3547-3563.

Hill, A. V. (1970). *First and Last Experiments in Muscle Mechanics.* Cambridge: Cambridge University Press.

Hoerner, S. F. (1965). *Fluid Dynamic Drag.* Midland Park, NJ. Published by the author.

Jenkins, F. A. and Shubin, N. H. (1998). Prosalirus bitis and the anuran caudopelvic mechanism. *J. Vert. Paleontol.* **18**, 495-510.

Johansson, L. C. and Lauder, G. V. (2004). Hydrodynamics of surface swimming in leopard frogs (*Rana pipiens*). *J. Exp. Biol.* **207**, 3945-3958.

Kargo, W. K. and Rome, L. C. (2002). Functional morphology of proximal hindlimb muscles in the frog *Rana pipiens*. *J. Exp. Biol.* **205**, 1987-2004.

Lauder, G. V., Madden, P. G., Mittal, R., Dong, H. and Bozkurttas, M. (2006). Locomotion with flexible propulsors: I. Experimental analysis of pectoral fin swimming in sunfish. *Bioinspir. Biomim.* **1**, S25-S34.

Lauder, G. V., Anderson, E. J., Tangorra, J. and Madden, P. G. A. (2007). Fish biorobotics: kinematics and hydrodynamics of self-propulsion. *J. Exp. Biol.* **210**, 2767-2780.

Lutz, G. J. and Rome, L. C. (1994). Built for jumping: the design of the frog muscular system. *Science* **263**, 370-372.

Nauwelaerts, S. and Aerts, P. (2003). Propulsive impulse as a covarying performance measure in the comparison of the kinematics of swimming and jumping in frogs. *J. Exp. Biol.* **206**, 4341-4351.

Nauwelaerts, S., Aerts, P. and D'Août, K. (2001). Speed modulation in swimming frogs. *J. Mot. Behav.* **33**, 265-272.

Nauwelaerts, S., Stamhuis, E. J. and Aerts, P. (2005). Propulsive force calculations in swimming frogs I. A momentum-impulse approach. *J. Exp. Biol.* **208,** 1435-1443.

Nauwelaerts, S., Ramsay, J. and Aerts, P. (2007). Morphological correlates of aquatic and terrestrial locomotion in a semi-aquatic frog, *Rana esculenta*: no evidence for a design conflict. *J. Anat.* **210**, 304-317.

Peplowski, M. and Marsh, R. (1997). Work and power output in the hindlimb muscles of Cuban tree frogs *Osteopilus septentrionalis* during jumping. *J. Exp. Biol.* **200**, 2861-2870.

Peters, S. E., Kamel, L. T. and Bashor, D. P. (1996). Hopping and swimming in the Leopard Frog, *Rana pipiens*: I. Step cycles and kinematics. *J. Morpho.* **230**, 1-16.

Quinn, G. P. and Keough, M. J. (2002). *Experimental Design and Data Analysis for Biologists.* Cambridge: Cambridge University Press.

Rand, S. A. (1952). Jumping ability of certain anurans, with notes on endurance. *Copeia* **1952**, 15-20.

Richards, C. T. (2008). The kinematic determinants of anuran swimming performance: an inverse and forward dynamics approach. *J. Exp. Biol.* **211**, 3181-3194.

Roberts, T. J. and Marsh, R. L. (2003). Probing the limits to muscle-powered accelerations: lessons from jumping bullfrogs. *J. Exp. Biol.* **206**, 2567-2580.

Shubin, N. H. and Jenkins, F. A. (1995). An early jurassic jumping frog. *Nature* **377**, 49-52.

Zug, G. R. (1978). Anuran locomotion-structure and function, **2**, jumping performance of semiaquatic, terrestrial and arboreal frogs. *Smithson Contrib. Zool.* **276**, 1-30.